

# JOURNAL OF SUSTAINABLE ENGINEERING AND TECHNOLOGY

Journal homepage: www.joset.com.ng

# Investigating the Effect of a Passenger Vehicle Front Profile on Aerodynamic Performance

Abubakar Isah<sup>1</sup>, Muhammad Uba Abdulazeez<sup>2</sup>, Mansur Aliyu<sup>3</sup>, Ibrahim Yahuza<sup>4</sup>

<sup>1,4</sup>Automotive Engineering Department, Faculty of Air Engineering, Air Force Institute of Technology Kaduna,

P.M.B 2104, Kaduna, Nigeria

<sup>2,3</sup>Department of Automotive Engineering, Faculty of Engineering and Engineering Technology, Abubakar Tafawa Balewa University Bauchi, P.M.B 0248, Bauchi, Nigeria
<sup>2</sup>Department of Mechanical Engineering, United Arab Emirates University

## **ARTICLE INFO**

Article History

Received: 13 Oct 2024 Accepted: 19 Dec 2024 Published: 18 April 2025

# **Corresponding Author:**

Abubakar Isah
Automotive Engineering
Department, Faculty of Air
Engineering, Air Force Institute of
Technology Kaduna, P.M.B 2104,
Kaduna, Nigeria
dankade@hotmail.com

## **ABSTRACT**

The design of a vehicle's aerodynamics is crucial for fuel efficiency. A vehicle with a body optimized to reduce drag typically achieves better fuel economy than a similar vehicle without aerodynamic enhancements. The drag coefficient, which is the measure of aerodynamic drag on a vehicle, is primarily influenced by how air flows around the vehicle, especially as air molecules stagnate at the front. This frontal pressure can be reduced by minimizing the vehicle's exposed frontal surface area, which can be evaluated through wind tunnel testing or Computational Fluid Dynamics (CFD) methods. This study used CFD analysis to examine the effect of a passenger vehicle's front hood angle on its aerodynamic performance. Simulations were performed using ANSYS Fluent 15.0, applying the Standard k-epsilon turbulence model, and the CAD models were developed using AutoCAD 2015. The results showed that adjusting the hood angle significantly reduced drag and lift coefficients by 7.72% and 33.3%, respectively, in head-on wind conditions. These modifications to the vehicle's front profile improved its stability and performance and enhanced fuel efficiency. This study highlights the importance of aerodynamics in vehicle design, demonstrating that even minor adjustments can lead to meaningful improvements. Additionally, it underscores the effectiveness of CFD, an effective tool for aerodynamic analysis, allowing engineers to optimize vehicle designs for better performance and environmental sustainability.

**Keywords**: Drag · Turbulence Models · Computational Fluid

Dynamics (CFD) · Lift · Fuel Economy

#### 1. Introduction

The rising ecological issues within the last decade and fuel prices triggered by the fuel crisis of the early 1970s necessitated a grave interest concerning the constant need for an improved fuel economy. For this reason, the requirement for the design and development of fuel-efficient vehicles has recently become stringent in the automobile industry [1]–[4]. The fuel efficiency of a vehicle is achievable either by increasing

its engine performance, reducing mass or by optimizing its body shape aerodynamically to reduce drag resistance [4], [5]. Nath et al. (2021) reported that fuel consumption due to aerodynamic drag consumes about half the vehicle's energy. Vignesh et al. (2019) viewed improving vehicle aerodynamic performance as the cheapest method to improve fuel efficiency and reduce emissions. Though the impact of vehicle drag is the most notable factor in vehicle aerodynamics, an aerodynamic lift also plays a quiet role in improving its dynamic stability. It has been found that the greater the vehicle lift, the higher the instability of the vehicle [7], [8]. Thus, apart from better fuel economy, an aerodynamically sound vehicle offers better ride stability and handling. These forces are primarily determined by the vehicle speed, frontal area, and drag and lift coefficients. They both increase proportionately with the square of the vehicle speed and thus, the lower the vehicle speed, the lower the force.

Many different vehicle body features describe its aerodynamic performance, and various techniques have been employed to investigate their effect. For instance, Dominy (2002) and Wang et al. (2017) mentioned that the front profile of a vehicle has the most significant contribution to drag, and by modifying it, there is a considerable decrease in drag. This is because, at first, the air struggles to flow around the vehicle, and when its molecules approach the car's front end, they stagnate. This pressure is seen lessened by decreasing the stagnation area at the front end. Also, by making the front end smooth, a continuous curve originating from the front bumper line permits the air molecules to pass smoothly. Chenyi (2021) in his study, he reported that Carr studied the influence of engine hood slope angles on the drag coefficient. The engine hood slope angle is the angle between the hood and the horizontal plane of the vehicle. The study plots the drag coefficient curve with different engine hood slope angles from 0° to 10° from the horizontal position. The results show a reduced drag with an increasing engine hood slope angle from 0° to 5°. However, the drag coefficient curve shows a nearly constant trend from 5° to 10°. In a similar vein, research involving simulation analysis of the aerodynamic properties of various two-dimensional car shapes by Guo et al. (2011) demonstrated that altering the front profile notably enhanced aerodynamic efficiency. The results revealed that the airflow stagnates at the front end of the bodywork and shrinks for the modified bodywork shape.

Overall, when investigating vehicle aerodynamic performance, the wind tunnel test is commonly a suitable means but is expensive, time-consuming and makes no flexible provision for future model modifications in the development process. As such, computational fluid dynamics (CFD) offers an alternative technique that has been in use since the 1960s. It is inexpensive and flexible, allowing for timely design modifications during development. To exemplify, Vignesh et al. (2019) investigated windscreen angle and hood inclination optimization for drag on a Proton Iswara car model using CFD at a velocity of 25 m/s. The drag coefficient was revealed to decrease linearly with an increase in hood angle from  $0^{\circ} - 20^{\circ}$ . They further performed an orthogonal experiment to estimate the effective drag. The results revealed that with combinations of 60° and 32° front and rear windscreen angles, respectively, and a hood inclination angle of 15°, the drag coefficient decreases by 27%. Recently, Chenyi (2021) performed an aerodynamic study using CFD on the vehicle shape parameters for two ground simulations on a DrivAer model. The original engine hood slope angle of the DrivAer model is 8° and was varied from 4° to 12°. The results showed drag and lift coefficient changes with different engine hood slope angles. The drag coefficient is slightly reduced with the enlarged hood angle. However, the lift coefficient is increased. Equating the similarity between the fixed and the moving ground, both drag and lift coefficients show a similar trend. So, the moving ground simulation has little impact on the results change when the engine hood angle is varied.

Therefore, this paper focused on performing a numerical investigation of the effect of front hood angle on the aerodynamic performance of a generic model of a passenger vehicle using CFD. An engine hood angle of 15° is considered for the generic vehicle model with the modified front profile.

# 2. Methodology

In this study, the generic passenger vehicle model was designed using AutoCAD 2015 software. The model was imported into ANSYS Fluent Design Modeller 15.0 software for the study. The investigation involves simulation in a virtual wind tunnel, a computational domain designed in the ANSYS Fluent interface. Tables 1 and 2 show the basic measurements of the generic vehicle model and the computational domain, respectively. Figure 1 presents the baseline passenger vehicle model produced for investigation, while Figure 2 shows the modified front profile model to minimize the overall drag and lift coefficients. Figure 3 shows the vehicle model in the computational domain designed for the simulation.

Table 1. Basic measurements of the generic passenger vehicle model

Section	Dimensions	
Wheelbase	3400 mm	
Height	1300 mm	
Front overhang	900 mm	
Rear overhang	1500 mm	
Wheel (r)	330.25 mm	
Width	2100 mm	
Engine hood angle	15°	

Table 2. Dimensions of the computational domain

Section	Dimensions
Length	14,500 mm
Height	3,000 mm
Width	4,100 mm

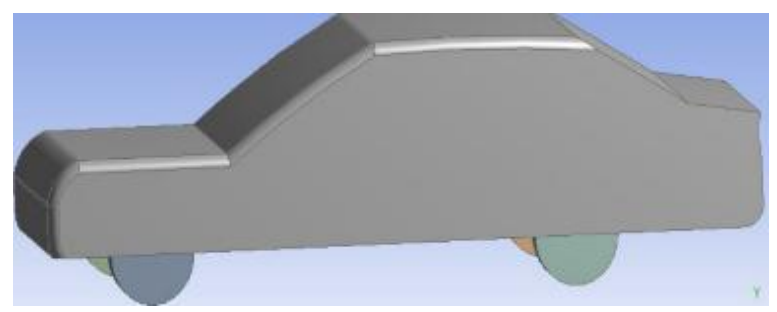


Figure 1. Baseline generic passenger vehicle model

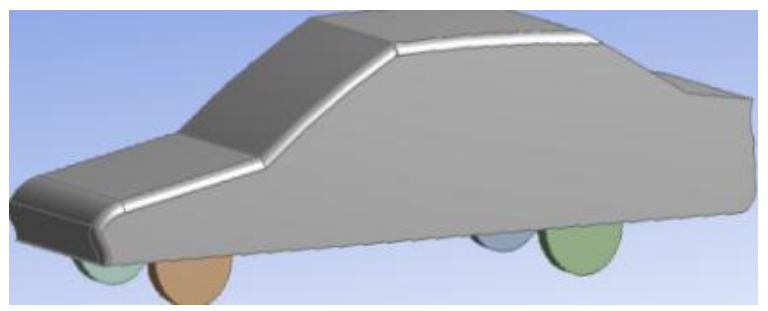


Figure 2. Modified generic passenger vehicle model

# 2.1 Steps of the Analysis

# a) Naming selection

The naming is done after the vehicle model is imported and the computational domain is designed. The face of the computational domain, 'inlet,' was selected and named "Velocity Inlet," and the face opposite was selected and named "Pressure Outlet" (see Figure 3). The model in the domain is called "Vehicle." The Symmetry planes are named "Symmetry," and the bottom and top surfaces are named "Road" and "Wall," respectively.

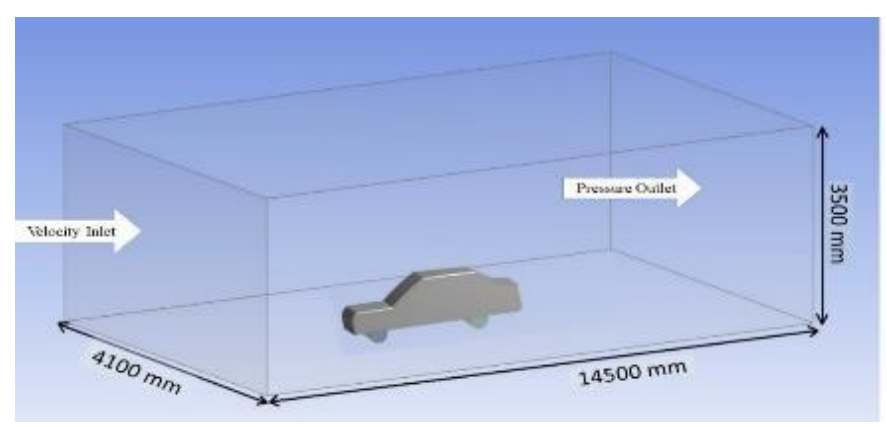


Figure 3. Passenger vehicle model in the computational domain

# b) Meshing option

Table 3 shows the meshing options used in this investigation. The surface unstructured mesh was performed on the model surfaces and the remaining unoccupied volume of the computational domain. Figures 4 and 5 present the mesh produced for the baseline model and the model with the trunk lip spoiler, respectively. The mesh generated consists of 56,578 nodes and 312,154 elements.

Table 3. Meshing options

Table 3. Meshing options			
Object name	Option		
State	Solved		
Physics preference	CFD		
Solver preference	Fluent		
Relevance centre	Fine		
Smoothing	High		
Span angle centre	Fine		

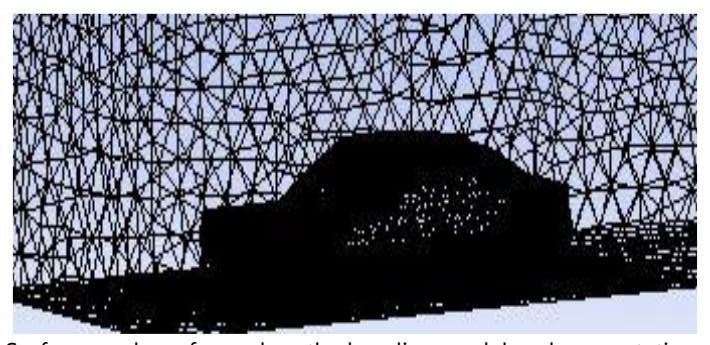


Figure 4. Surface mesh performed on the baseline model and computational domain

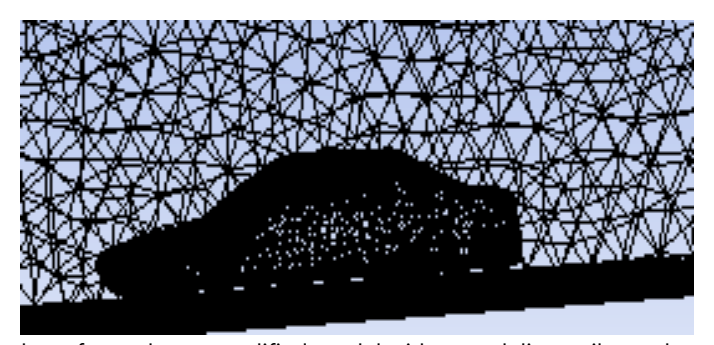


Figure 5. Surface mesh performed on a modified model with a trunk lip spoiler and computational domain

## c) Simulation setup

The "Double Precision" was carefully chosen to perform the simulation. A pressure-based solver was considered primarily for low-speed incompressible flow. The standard  $k-\varepsilon$  turbulence model was selected as

one of the most commonly used Reynolds Average Navier-Stokes (RANS) turbulence models, which suit the workhorse of practical engineering flow calculations [13]. The ANSYS Fluent CFD solver uses the Navier-Stokes equations, composed of continuity and momentum on average, Eqn. 1 and 2, respectively.

$$\frac{\partial \rho}{\partial t} + \frac{\partial}{\partial X_i} (\rho u_i) = 0 \tag{1}$$

$$\frac{\partial}{\partial t}(\rho u_i) + \frac{\partial}{\partial x_i}(\rho u_i u_j) = \frac{\partial \rho}{\partial x_i} + \frac{\partial}{\partial x_j} \left[ \mu \left( \frac{\partial u_i}{\partial x_j} + \frac{\partial u_j}{\partial x_i} - \frac{2}{3} \delta_{ij} \frac{\partial u_i}{\partial x_i} \right) \right] + \frac{\partial}{\partial x_i} \left( -\rho \overline{u_i} \underline{u_j} \right)$$
(2)

Equation 2 is the RANS equation, where u,  $\rho$  and  $\mu$  represent the velocity, density and dynamic viscosity of the fluid. The term,  $\left(-\rho \overline{u_i} u_j\right)$  in the equation, a tensor accounts for the turbulent fluctuations. It is known as the specific Reynolds stress tensor that is required to be modelled to close the RANS equation [14], [15]. Modelling turbulence is a computational procedure requiring some approximations in the governing differential equations to obtain a solution. The various types of approximation for computing the turbulence in the flow are known as turbulence models, some of which employ the Boussinesq hypothesis to relate the Reynolds stress and mean velocity (Aftab et al., 2016). For turbulent flows, as reported by Yakhot (1992) (as cited in [16]), the Standard k-epsilon turbulence model applies:

$$\frac{\partial}{\partial t}(\rho k) + \frac{\partial}{\partial x_i}(\rho k u_i) = \frac{\partial}{\partial x_j} \left[ \left( \mu + \frac{\mu_t}{\sigma_k} \right) \frac{\partial k}{\partial x_i} \right] + G_k + G_b + \rho \varepsilon + Y_M + S_k$$
 (3)

$$\frac{\partial}{\partial t}(\rho \varepsilon) + \frac{\partial}{\partial x_i}(\rho \varepsilon u_i) = \frac{\partial}{\partial x_i} \left[ \left( \mu + \frac{\mu_t}{\sigma_{\varepsilon}} \right) \frac{\partial \varepsilon}{\partial x_i} \right] + C_{1\varepsilon} \frac{\varepsilon}{k} + (G_k + C_{3\varepsilon} G_b) - C_{2\varepsilon} \rho \frac{\varepsilon^2}{k} + S_{\varepsilon}$$
(4)

In these Eqns. 3 and 4,  $G_k$  and  $G_b$  represents the generation of turbulence kinetic energy due to the mean velocity gradients and buoyancy.  $Y_M$  represents the contribution of the fluctuating dilatation incompressible turbulence to the overall dissipation rate.  $C_{1\varepsilon}$ ,  $C_{2\varepsilon}$ , and  $C_{3\varepsilon}$  are constant.  $\sigma_k$  and  $\sigma_{\varepsilon}$  are the turbulent Prandtl numbers for k and  $\varepsilon$  respectively.  $S_k$  and  $S_{\varepsilon}$  are user-defined source terms. The turbulent viscosity,  $\mu_t$  is computed by combining k and  $\varepsilon$ , Eqn. 5 as follows:

$$\mu_t = \rho C_\mu \frac{k^2}{s} \tag{5}$$

where  $C_{\mu}$  is a constant.

The model constant  $C_{1\varepsilon}$ ,  $C_{2\varepsilon}$ ,  $C_{\mu}$ ,  $\sigma_k$  and  $\sigma_{\varepsilon}$  have the following widely accepted values determined from experiments, although someone can change them if needed:

$$C_{1\varepsilon} = 1.44, C_{2\varepsilon} = 1.92, C_{u} = 0.09, \sigma_{k} = 1.0, \text{ and } \sigma_{\varepsilon} = 1.3$$

The production of turbulence kinetic energy,

$$G_k = \frac{\partial u_j}{\partial x_i} \left( -\rho \overline{u_i u_j} \right) \tag{6}$$

To evaluate  $G_k$  in a manner consistent with the Boussinesq hypothesis,

$$G_k = \mu_t S^2 \tag{7}$$

where S is the modulus of the mean rate-of-strain tensor, defined as

$$S \equiv \sqrt{2S_{ij}S_{ij}} \tag{8}$$

It is noteworthy that the assumption of the Standard  $k - \varepsilon$  turbulence model is that the flow is fully turbulent, and the effects of molecular viscosity are negligible. Thus, the model is valid for fully turbulent flows. The relationship between drag and lift forces is given in Eqn. 9 and 10, respectively, as obtained in [17] and [18]. The lift force is the force that reduces the tyre ground adhesion, acting perpendicular to the vehicle. The

drag force is the force acting relative to the direction of motion of the vehicle to the surrounding fluid and is essential in determining a vehicle's fuel consumption.

$$C_d = \frac{F_d}{0.5\rho V^2 A} \tag{9}$$

$$C_l = \frac{F_l}{0.5\rho V^2 A} \tag{10}$$

where  $F_d$  and  $F_l$  are the drag and lift forces,  $C_d$  and  $C_l$  are the coefficients of drag and lift,  $\rho$  is the density of the air, A is the frontal area of the vehicle, and V is the relative speed. The drag and lift coefficients are valuable when equating the aerodynamic efficiency of different vehicles. Table 4 presents the viscous and turbulence model settings carefully chosen for this investigation.

Table 4. Viscous and turbulence model settings

Turbulent model	k-epsilon
k-epsilon	Standard
Near wall treatment	Enhance wall function
Operating conditions	Ambient

# d) Boundary condition setting

The boundary conditions employed in this research involved the inlet velocity, which was 40 m/s, which is the velocity of the model at which it is moving. The surrounding air was assumed to be incompressible. The pressure (gauge) at the outlet was considered to act in the direction perpendicular to the boundary.

#### e) Solution method and control

The lift and drag monitors were produced from the "Monitors" section, in which their convergence values were determined during the iterations. Table 5 presents the monitoring and convergence criteria set for this investigation.

Table 5. Monitoring and Convergence criteria

Equations	Flow and Turbulence
Monitor	Residuals, Lift and Drag coefficients
Convergence criteria	Continuity, epsilon, k, x, and y- direction = 0.0001 respectively

The Coupled scheme was considered, which solves the momentum equation and pressure as coupled, leading to quicker convergence, a more sensible and secure method [19]. Selections for "Spatial Discretization" are made sequentially in which the Gradient was chosen to be "Least Square Cell-Based," the "Pressure" to be 'Standard', the 'Momentum', Turbulent Kinetic Energy' and 'Turbulent Dissipation Rate' to be in 'Second Order Upwind' respectively.

# f) Solution initialization and running the calculations

The setup was initialized using hybrid initialization, and the calculations were set to run for 400 iterations from the specified boundary conditions. Hybrid Initialization is a collection of recipes and boundary interpolation methods. It solves the Laplace equation to produce a velocity field that conforms to complex domain geometries and a pressure field that smoothly connects high and low-pressure values in the CD. All other variables (that are temperature, turbulence, species, and so on) will be patched based on domain averaged values or a predetermined recipe [20].

#### 3. Results and Discussion

This section presents the analysis results of two different configurations. Specifically, Figures 6 and 7 depict the static pressure contours on the model's surface. Figure 6 represents the model with an unmodified

front profile, while Figure 7 illustrates pressure contours on the surface of the modified model. These visual representations compare the two configurations and their respective static pressure distributions.

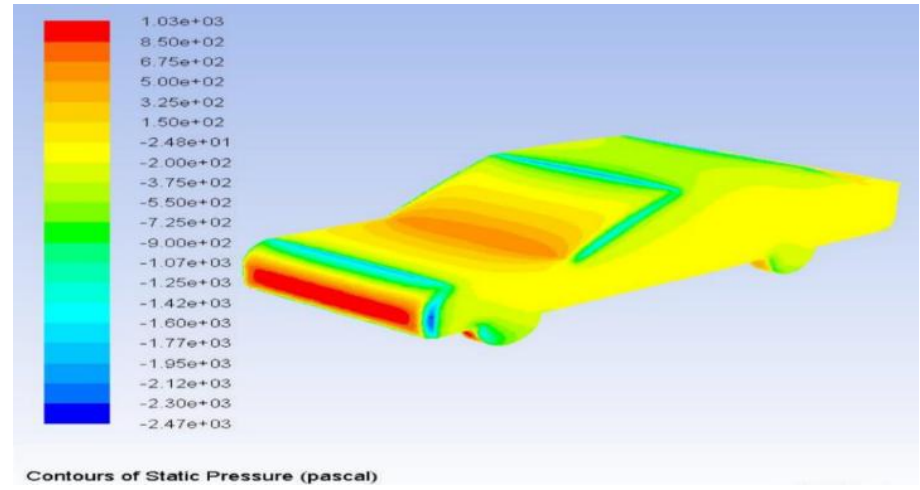


Figure 6. Static pressure contour on the surface of the unmodified front profile model

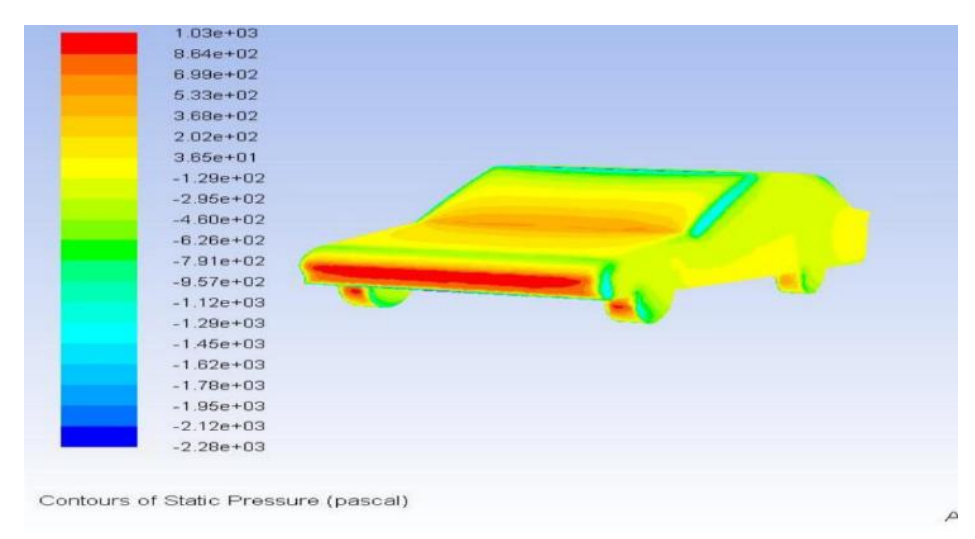


Figure 7. Static pressure contour on the surface of the modified front profile model

Figures 8 and 9 present the velocity vectors on the surface of unmodified and modified models, respectively.

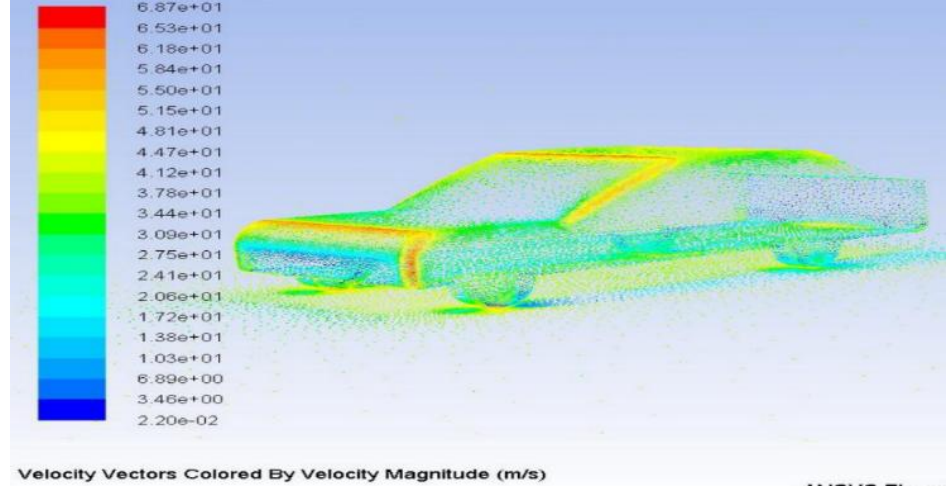


Figure 8. Velocity vectors on the surface of the unmodified front profile model

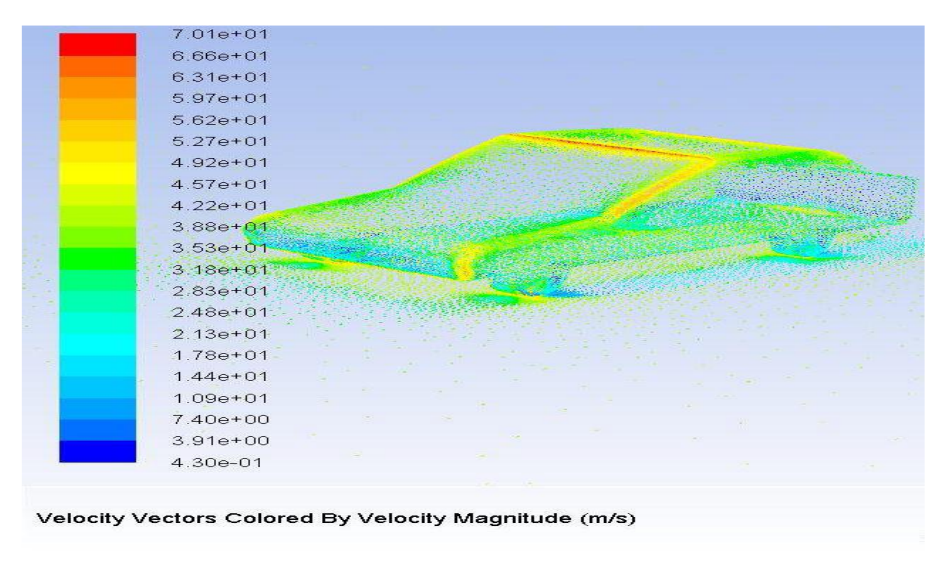


Figure 9. Velocity vectors on the surface of the modified front profile model

When examining the static pressure contours on the surfaces of the two models, it is evident from Figures 6 and 7 that the maximum pressure obtained is consistent at  $1.03 \times 10$ . However, a closer analysis reveals that the maximum pressure for the unmodified and modified models, depicted in Figures 8 and 9, differs slightly at 68.7 m/s and 70.1 m/s, respectively. Figure 6 highlights a higher pressure exerted at the unmodified model's cowl top than Figure 7 of the modified model, reaching a maximum pressure of  $6.75 \times 10^2$  pascals and  $5.33 \times 10^2$  pascals, respectively. A notable observation is the increased pressure exerted on the front end of the unmodified model in Figure 6 compared to the modified front end in Figure 7, owing to the reduction in the front surface area exposed to the free stream. For a comprehensive overview, Table 4 provides a detailed summary of the comparative results obtained for the drag and lift coefficients of the two models.

Table 4. Coefficients of drag and lift

Configurations	Cď	Cl
Unmodified model front profile	0.337	0.120
Modified model front profile	0.311	0.080

The results presented proved that drag reduction, as well as lift force, is attainable by modifying the front profile of a vehicle. As revealed in Table 4 before the modification, the drag coefficient obtained was 0.337, and the lift coefficient was 0.120. However, after the modification, there is a reasonable reduction in the drag and lift coefficient. These coefficients were obtained to be 0.311 and 0.080, respectively. A similar effect is seen in the studies carried out by [11] and [6] respectively. This achievement proved that modifying the front-end profile reduced the static pressure developed at the vehicle's front end. This alone is due to the reduction in the front-end surface area that contributes much to its aerodynamic performance, as shown in Figures 6 and 7. Besides, the significant decrease in lift coefficient indicated that the modified model exerted greater downforce to hold the vehicle rather than lift it onto the ground. This is in agreement with the study carried out in [12] Based on simulation analysis of aerodynamic characteristics of different two-dimensional automobile shapes, the modified model will have more excellent dynamic stability than the unmodified model. Comparing the velocity vectors, Figs 8 and 9, on the surfaces of the two models at the point where flow separation occurs, the velocity at which the airflow happens to be at a maximum at these points.

# 4. Conclusion

This study investigated the impact of a passenger vehicle's front profile on its aerodynamic performance. The analysis demonstrated that modifying the front profile significantly improves fuel efficiency by reducing the drag while affecting the stability performance of the vehicle by lowering the lift coefficients. The results also indicated that the model with the modified front profile exhibited superior aerodynamic characteristics. Additionally, the values obtained from the study provided valuable insights into the vehicle's

behavior at a speed of 144 km/h. Finally, the CFD method used in this analysis proved effective for aerodynamic evaluation, allowing for straightforward modification of the vehicle model.

#### References

- [1] P. Vinayagam, M. Rajadurai, K. Balakrishnan, and G. M. Priya, "Design modification on Indian Road Vehicles to Reduce Aerodynamic Drag," *Int. J. Adv. Eng. Manag. Sci.*, vol. 3, no. 8, pp. 6–11, 2017, doi: 10.24001/ijaems.3.8.6.
- [2] C. Radhakrishnan, K. Yokeshwaran, N. Karunaraja, A. N. G, D. M. K. R, and M. Gowtham, "CFD Analysis of a FSAE Car Equipped with Front and Rear Wings," *Int. J. Innov. Res. Sci. Eng. Technol.*, vol. 5, no. 4, pp. 5573–5582, 2016, doi: 10.15680/IJIRSET.2016.0504193.
- [3] M. N. Sudin, M. A. Abdullah, S. A. Shamsuddin, F. R. Ramli, and M. Mohd, "Review of Research on Vehicles Aerodynamic Drag Reduction Methods," *Int. J. Mech. Mechatronics Eng. IJMME-IJENS*, vol. 14, no. 02, pp. 35–47, 2014.
- [4] B. Datta, V. Goel, S. Garg, and I. Singh, "Study of Various Passive Drag Reduction Techniques on External Vehicle Aerodynamics Performance: CFD Based Approach," *Int. Res. J. Eng. Technol.*, vol. 06, no. 05, pp. 1851–1871, 2019.
- [5] D. S. Nath, P. C. Pujari, A. Jain, and V. Rastogi, "Drag reduction by application of aerodynamic devices in a race car," *Adv. Aerodyn.*, vol. 3, no. 4, pp. 1–20, 2021, doi: 10.1186/s42774-020-00054-7.
- [6] S. Vignesh, V. S. Gangad, V. Jishnu, A. Krishna, and Y. S. Mukkamala, "Windscreen angle and Hood inclination optimization for drag," *Procedia Manuf.*, vol. 30, pp. 685–692, 2019, doi: 10.1016/j.promfg.2019.02.062.
- [7] J. Abinesh and J. Arunkumar, "CFD Analysis of Aerodynamic Drag Reduction and Improve Fuel Economy," *Int. J. Mech. Eng. Robot. Res.*, vol. 3, no. 4, pp. 430–440, 2014.
- [8] J. Howell, S. Windsor, and M. Passmore, "Some Observations on Shape Factors Influencing Aerodynamic Lift on Passenger Cars," *fluids*, vol. 6, no. 44, pp. 1–16, 2021, doi: 10.3390/fluids6010044 Received:
- [9] R. Dominy, "An Introduction to Modern Vehicle Design," in *Body design: Aerodynamics*, First., J. Happian-Smith, Ed. Butterworth-Heinemann, 2002, pp. 111–124.
- [10] Q. Wang, Z. Wu, X. Zhu, L. Liu, and Y. Zhang, "Analysis of Aerodynamic Performance of Tesla Model S by CFD," in 3rd Annual International Conference on Electronics, Electrical Engineering and Information Science (EEEIS 2017), 2017, vol. 131, no. Eeeis, pp. 16–21.
- [11] Z. Chenyi, "Aerodynamic Study on the Vehicle Shape Parameters with Respect to Ground Simulation," Wissenschaftliche Reihe Fahrzeugtechnik Universität Stuttgart, 2021. doi: 10.1007/978-3-658-33439-0\_1.
- [12] L. X. Guo, Y. M. Zhang, and W. J. Shen, "Simulation analysis of aerodynamics characteristics of different two-dimensional automobile shapes," *J. Comput.*, vol. 6, no. 5, pp. 999–1005, 2011, doi: 10.4304/jcp.6.5.999-1005.
- [13] J. Levin and R. Rigdal, "Aerodynamic analysis of drag reduction devices on the underbody for SAAB 9-3 by using CFD," Chalmers University of Technology, 2011.
- [14] S. M. A. Aftab, A. S. M. Rafie, N. A. Abdul Razak, and K. A. Ahmad, "Turbulence model selection for low reynolds number flows," *PLoS One*, vol. 11, no. 4, pp. 1–15, 2016, doi: http://dx.doi.org/10.1371/journal.pone.0153755.
- [15] A. Altememe, O. J. Myers, and A. Hall, "Computational Fluid Dynamic Analysis of Flapping Wing of Micro Aerial Vehicle at Very Low Reynolds Numbers Turbulent Flow," *Int. J. Aeronaut. Aerosp. Eng. Res.*, vol. 1, no. 2, pp. 68–75, 2019, doi: http://dx.doi.org/10.18689/ijae-1000110.
- [16] G. J. Hortelano-Capetillo, J. L. Martínez-Vázquez, J. MercedZuñiga- Cerroblanco, and G. Rodriguez-Ortiz, "Analysis of drag and lift forces for a sedan car using a rear lip spoiler," *J. Mech. Eng.*, vol. 4, no. 13, pp. 23–31, 2020, doi: 10.35429/JME.2020.13.4.23.31.
- [17] D. Vishal, J. Tanuj, and S. Gurminder, "Effect of Front Slant Angle on Aerodynamics of a Car," in *Advances in Engineering Design*, A. Prasad, S. S. Gupta, and R. K. Tyagi, Eds. Springer Nature Singapore Pte Ltd, 2018, pp. 641–653. doi: 10.1007/978-981-13-6469-3\_59.
- [18] C. Bayındırlı and M. Çelik, "The determination of effect of windshield inclination angle on drag coefficient of a bus model by CFD method," *Int. J. Automot. Eng. Technol.*, vol. 9, no. 3, pp. 122–129,

2020.

- [19] R. S. Gondipalle, "CFD Analysis of the Under Hood of a Car for Packaging Considerations," Clemson University, 2011.
- [20] ANSYS Inc, "ANSYS Fluent Theory Guide," vol. 15317, no. November. SAS IP, Inc. U.S.A, pp. 724–746, 2013.